

Synthesis, Structure, Properties, and Applications of Bimetallic Nanoparticles of Noble Metals

Kateryna Loza,* Marc Heggen,* and Matthias Eppe*


Bimetallic nanoparticles of noble metals are of high interest in imaging, biomedical devices, including nanomedicine, and heterogeneous catalysis. Synthesis, properties, characterization, biological properties, and practical applicability of nanoparticles on the basis of platinum group metals and the coin metals Ag and Au are discussed, also in comparison with the corresponding monometallic nanoparticles. In addition to the parameters that are required to characterize monometallic nanoparticles (mainly size, size distribution, shape, crystallographic nature, surface functionalization, charge), further information is required for a full characterization of bimetallic nanoparticles. This concerns the overall elemental composition of a bimetallic nanoparticle population (ratio of the two metals) and the internal distribution of the elements in individual nanoparticles (e.g., the presence of homogeneous alloys, core-shell systems, and possible intermediate stages). It is also important to ensure that all particles are identical in terms of elemental composition, that is, that the homogeneity of the particle population is given. Macroscopic properties like light absorption, antibacterial effects, and catalytic activity depend on these properties. The currently available methods for a full characterization of bimetallic nanoparticles are discussed, and future developments in this field are outlined.

1. Introduction

Nanoparticles of noble metals have been prepared and studied since decades. They have established themselves as valuable materials in various applications, for example, homogeneous and heterogeneous catalysis, nanomedicine, and imaging.^[1]

Dr. K. Loza, Prof. M. Eppe
Inorganic Chemistry and Center for Nanointegration
Duisburg-Essen (CeNIDE)
University of Duisburg-Essen
45117 Essen, Germany
E-mail: kateryna.loza@uni-due.de; matthias.eppe@uni-due.de

Dr. M. Heggen
Ernst Ruska-Center for Microscopy and Spectroscopy with Electrons
Forschungszentrum Jülich GmbH
52425 Jülich, Germany
E-mail: m.heggen@fz-juelich.de

 The ORCID identification number(s) for the author(s) of this article can be found under <https://doi.org/10.1002/adfm.201909260>.

© 2020 The Authors. Published by WILEY-VCH Verlag GmbH & Co. KGaA, Weinheim. This is an open access article under the terms of the Creative Commons Attribution-NonCommercial-NoDerivs License, which permits use and distribution in any medium, provided the original work is properly cited, the use is non-commercial and no modifications or adaptations are made.

DOI: 10.1002/adfm.201909260

The methods for their synthesis have been refined to a very high degree, including a control over particle size and shape.^[1g,2] Bimetallic nanoparticles have been introduced later but are now an exciting area of research because they offer a new degree of freedom to vary the particle properties by blending two metals in one particle. This extends their applicability in catalysis (including electrocatalysis), biomedicine, and imaging.^[2d,3] Here, we discuss the current state of the art of bimetallic nanoparticles. We will focus on bimetallic nanoparticles that contain noble metals, that is, platinum group metals and the two noble coin metals silver (Ag) and gold (Au).

2. Synthesis of Bimetallic Nanoparticles

Generally, there are two methods to prepare nanoparticles: bottom-up (by reduction of the metal cations) and top-down (by disassembling larger objects, for example, by laser ablation or grinding).^[1g,2b,4] We will consider them subsequently.

The bottom-up method requires a suitable soluble source of metals, usually metal cations in the form of soluble salts or coordinated by suitable ligands. To such a solution, a reducing agent is added whose nature has a strong influence on the particle properties. Numerous methods have been developed where reducing agents like glucose, citrate, or sodium borohydride are applied. A special case is the so-called polyol method where the solvent is a high-boiling alcohol that at the same time serves as reducing agent. The particle growth and the colloidal stability are usually controlled by suitable capping agents like surfactants, polymers, and polyelectrolytes. The nature of the resulting nanoparticles depends on various parameters like temperature, time, and reagent concentrations. Often, these cannot be fully controlled to obtain monodisperse nanoparticle populations. After all, the underlying processes of nucleation and crystal growth are complex and still insufficiently understood.^[5]

In the synthesis of bimetallic nanoparticles, at least two metal sources must be used (example: Ag⁺ and Au³⁺).^[6] Their presence during the reduction determines the nature of the resulting bimetallic nanoparticles. If both metal precursors are present at the same time, their simultaneous reduction may lead to alloyed nanoparticles where both metals (example: Ag, Au) are present in a statistical mixture. In contrast, a sequential reduction ("seeded growth") can lead to core-shell particles.^[4c,7]

For example, if Au^{3+} is reduced first to gold nanoparticles, the subsequent addition of Ag^+ in the presence of a sufficient amount of reducing agent leads to bimetallic particles with a gold core and a silver shell. This happens because gold is nobler than silver. The reverse case is not always possible. Suppose that Ag^+ is reduced first to silver nanoparticles, followed by the addition of Au^{3+} . In that case, cations of the nobler gold will oxidize the metallic silver and be deposited on the surface of the dissolving silver nanoparticle. This can lead to a hollow gold nanoparticle where the silver core has been completely dissolved.^[7a,8] To constrain this oxidative dissolution of the less noble metal, one can add an excess of stronger reducing agents together with the nobler metal ion. However, experience shows that it is not always possible to control redox chemistry on the nanoscale in such a complex reaction mixture.

The most controllable top-down method is laser ablation. Here, a solid target (in this case, a bimetallic alloy) is treated with a laser beam. At suitable conditions, well-dispersed bimetallic nanoparticles are obtained which can then be further fractionized and surface-functionalized.^[3a,9] Another option is a two-step synthesis, that is, a laser irradiation of a mixture of silver and gold nanoparticles.^[10] **Figure 1** illustrates the basic synthetic concepts.

3. Structural Features of Bimetallic Nanoparticles

In general, the average particle size and the particle size distribution are the most important properties of nanoparticles. However, these parameters are not always easy to define and to determine, given the fact that most particle dispersions do not consist of completely uniform particles. Different particle size determination methods are based on different physical principles and can lead to different results.^[11] First of all, one has to distinguish between methods that probe dispersed particles (like dynamic light scattering, centrifugation techniques, nanoparticle tracking analysis) and methods that probe only the solid (metallic) core. In dispersion, the hydrodynamic particle diameter is measured, and the primary particles may also be agglomerated. In the dried (solid) state, the primary particle size is measured, but usually this does not permit a conclusion about the situation in the dispersed state because particles often agglomerate during drying. This is frequently the case in electron microscopy where dried samples are studied.

Particle size determination methods are usually applied to dispersed nanoparticles in the colloidal state. By probing different physical effects, they give information on average particle diameters and the particle size distribution. They can be applied to bimetallic nanoparticles in the same way as to monometallic nanoparticles, with all given limitations. The most common techniques are dynamic light scattering (DLS), analytical ultracentrifugation (AUC), disc centrifugal sedimentation (DCS), and nanoparticle tracking analysis (NTA), based on the Brownian motion of the particles.^[11a–d] Less frequently applied are static light scattering (SLS),^[12] small-angle X-ray scattering (SAXS),^[11d,13] asymmetric field flow fractionation (AFFF),^[14] and electrophoresis.^[15] Note that in some cases (especially with centrifugation methods), the particle density must be known which for bimetallic nanoparticles depends on the actual



Kateryna Loza studied physics at the V. N. Karazin Kharkiv National University (Ukraine). After the completion of her doctoral studies in 2016, she worked on the ultrastructural characterization of bimetallic nanoparticles in the groups of Prof. M. Epple, University of Duisburg-Essen, Dr. M. Heggen, the Ernst Ruska-Centre for Microscopy and Spectroscopy with Electrons, Forschungszentrum Jülich, and Prof. K. Kaneko, Kyushu University (Japan). Since 2019, she has been a staff scientist at the University of Duisburg-Essen. Her main research interests are nanomaterials and their fate in biological media, the physicochemical characterization of nanosized objects, and electron microscopy.



Marc Heggen studied physics at the RWTH Aachen and obtained his doctorate with Prof. K. Urban in 2003. He did post-doctoral research at the Ecole des Mines (Nancy) and at Harvard University (Cambridge, MA). Since 2013, he has been a staff scientist at the Ernst Ruska Centre, Forschungszentrum Jülich, and the head of the Catalysis group (since 2017). His main research interests are nanomaterials, nanoparticle catalysts for energy conversion, aberration-corrected electron microscopy, and the physics of structurally complex intermetallic alloys.



Matthias Epple studied chemistry at the Technical University of Braunschweig. After obtaining his Ph.D. there in 1992, he went to the University of Washington (Seattle, USA) and the Royal Institution (London, UK) for post-doctoral studies. He obtained his habilitation at the University of Hamburg in 1997 and became associate professor of Inorganic Chemistry at the Ruhr-University of Bochum in 2000. Since 2003, he has been a full professor of Inorganic Chemistry at the University of Duisburg-Essen. His research interests comprise biomaterials, biomineralization, as well as the synthesis and structural characterization of nanoparticles.

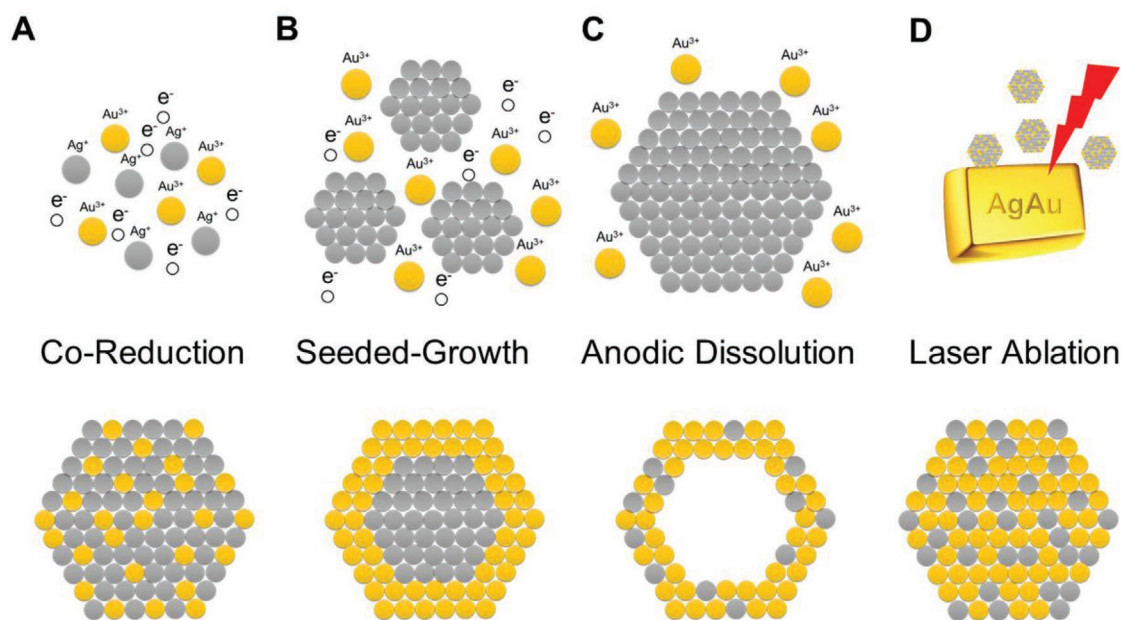


Figure 1. Synthesis of alloyed bimetallic nanoparticles in the silver–gold system (“electrum”) as examples in schematic representations. A) Bottom-up synthesis, leading to alloyed silver–gold nanoparticles after co-reduction. B) Bottom-up synthesis, leading to silver–gold core–shell nanoparticles (seeded-growth mechanism). C) Bottom-up synthesis, leading to hollow gold nanoshells (anodic dissolution of the silver core). D) Top-down synthesis to prepare alloyed silver–gold nanoparticles from an alloyed target by laser ablation.

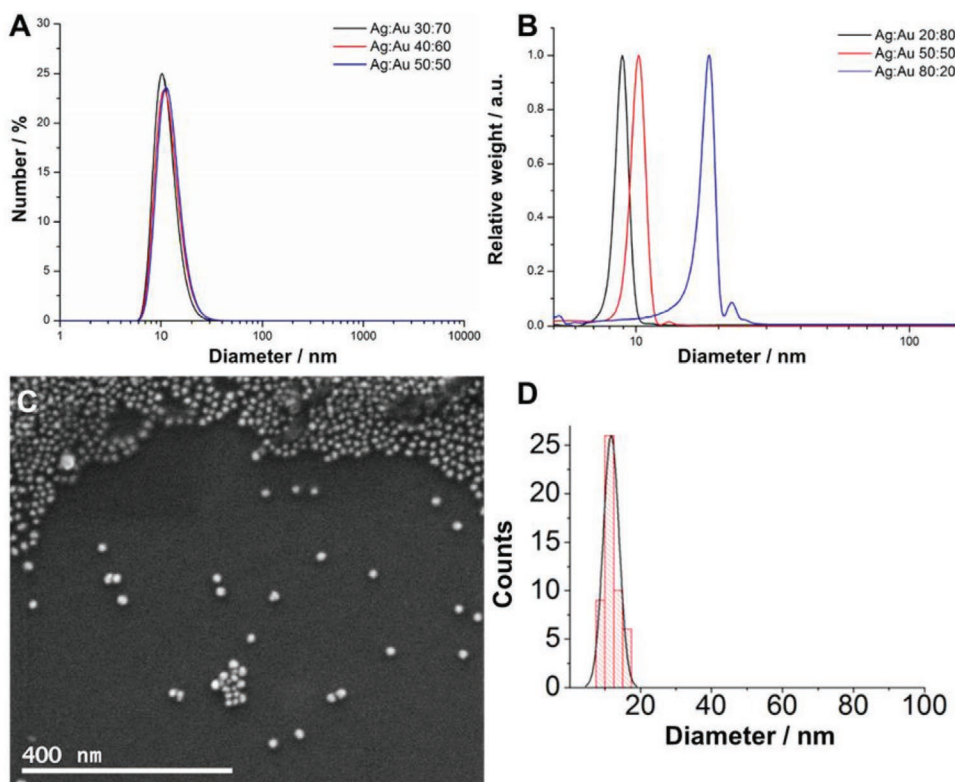


Figure 2. Analytical results of different bimetallic silver–gold nanoparticles in dispersion (DLS and DCS) and in the solid state (SEM): A) dynamic light scattering, B) disc centrifugal sedimentation, C) SEM image of bimetallic silver–gold 50:50 nanoparticles, and D) particle size distribution derived from these SEM data. Reproduced with permission.^[16] Copyright 2014, Simon Ristig.

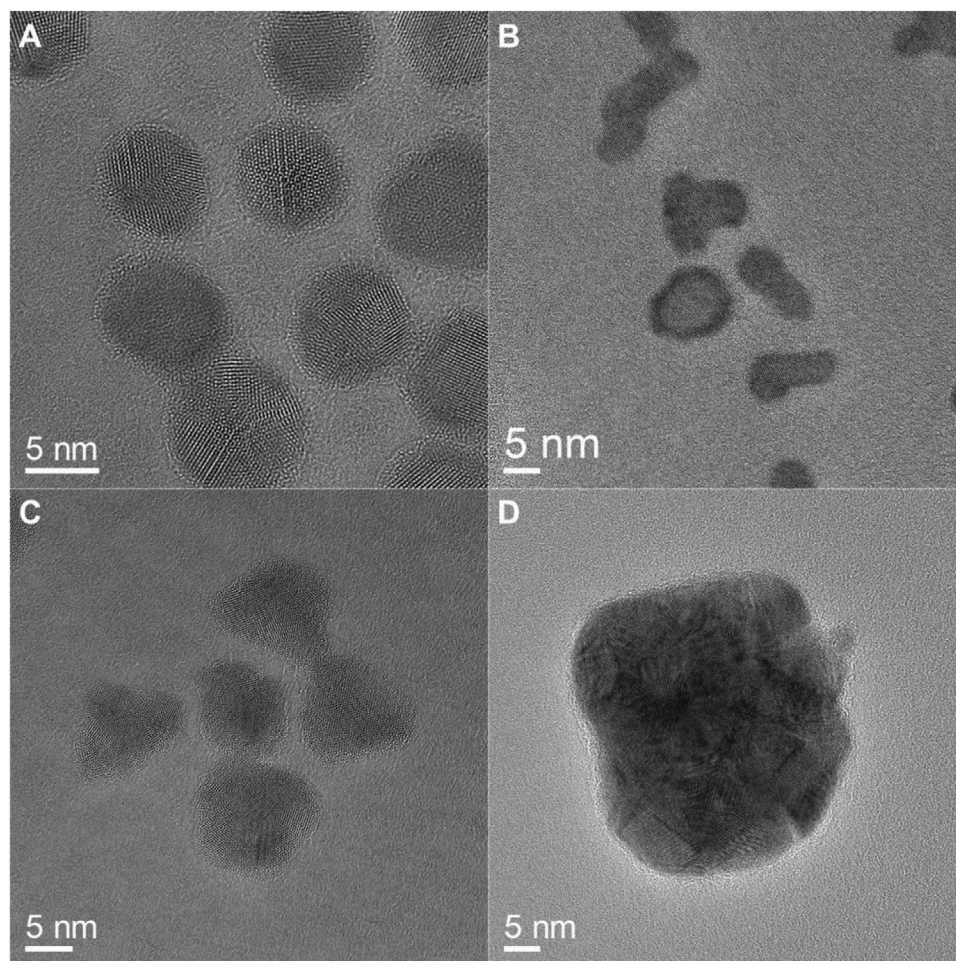


Figure 3. Representative HRTEM images of bimetallic nanoparticles: A) Twinned gold–palladium nanoparticles, B) hollow silver–platinum nanoparticles, C) intergrown palladium–platinum nanoparticles, and D) a larger multiply-twinned silver–gold nanoparticle. Reproduced with permission.^[18,19] Copyright 2018, 2019, Kateryna Loza.

particle composition. This information is available only from elemental analysis on both macro- and microscale. **Figure 2** shows some typical analytical results for dispersed bimetallic nanoparticles.

Without electron microscopy in combination with high-end spectroscopic techniques, a meaningful analysis of bimetallic nanoparticles is impossible. For larger nanoparticles (>10 nm), scanning electron microscopy (SEM) may be sufficient, but usually (high-resolution) transmission electron microscopy (TEM or HRTEM) is required to shed light on particle size and shape. Electron diffraction helps to identify crystalline domains and the crystal structure in general. However, it must be stressed that the “small world” within an electron microscopic image must always be complemented by methods that probe a statistically more relevant part of a sample.

As with monometallic nanoparticles, high-resolution transmission electron microscopy and electron diffraction have revealed that many nanoparticles consist of more than one crystalline domain. This feature appears to result from very early nucleation steps, that is, the initial nucleus is already twinned and preserves this feature during growth.^[17] Thus, a thorough analysis of the crystalline nature of a nanoparticle permits us to draw conclusions about the very first (and non-analyzable)

nucleus. Electron microscopy can also demonstrate the presence of hollow or intergrown (fused) particles. **Figure 3** shows typical results from electron microscopy.

A supplementary method to analyze polycrystalline nanoparticles is X-ray powder diffraction (XRD).^[13d,20] Its advantage lies in the fact that billions of particles are probed at the same time, unlike the situation in electron microscopy. This is a more representative part of a sample, but on the other hand, all results show the average of many particles and individual differences inside a sample are often overlooked. Therefore, it conveniently complements electron microscopy. By analysis of diffraction peak profiles, the size of the crystalline domains can be computed, together with an assessment of the internal microstrain.^[20d,21] X-ray powder diffraction can be applied if the crystalline domains are larger than about 2–3 nm. The peak broadening that occurs with smaller crystallites can be quantitatively evaluated by quantitative Rietveld refinement. The presence of intermetallic alloys can be detected by measuring the lattice parameters. Usually (but not always), an alloy will observe Vegard’s rule, that is, it will have intermediate lattice parameters compared to the pure metals.^[21a,22] X-ray diffractions reaches a limit when the crystalline domains become too small. In that case, the peaks will be too broad for evaluation.

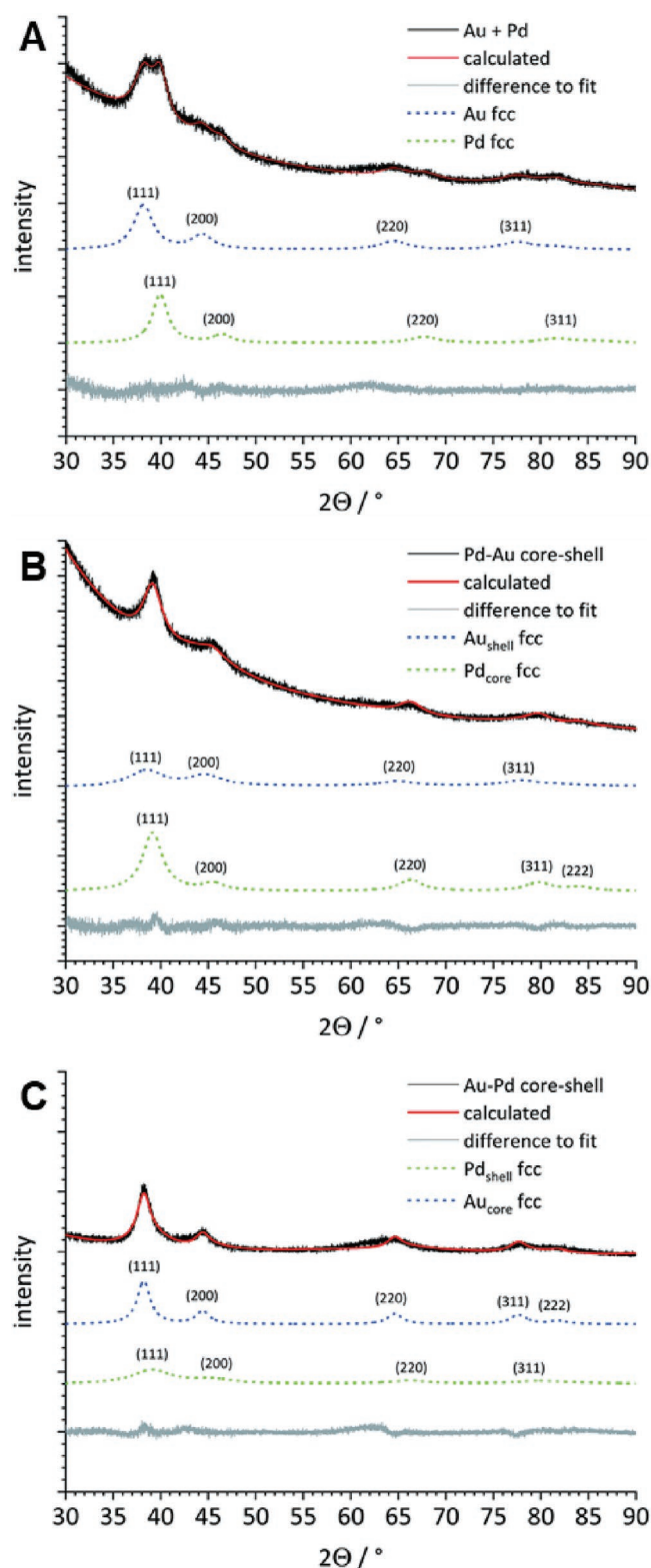


Figure 4. X-ray powder diffractometry to analyze bimetallic Au-Pd nanoparticles. A) Physical mixture of monometallic gold and palladium nanoparticles (8 nm) where both metals can be distinguished by Rietveld refinement. B) In Pd-Au core-shell nanoparticles, the palladium core (5–6 nm) can be distinguished from the gold shell (1–2 nm). C) Vice versa, in Au-Pd core-shell nanoparticles, the gold core (5–6 nm) can be

Unfortunately, for metallic nanoparticles that crystallize in high-symmetry lattices like body-centered cubic (bcc), cubic-close packing/face-centered cubic (ccp/fcc), or hexagonal-close packing (hcp), there is often a shortage of diffraction peaks that prevents a meaningful analysis. On the other hand, anisotropic crystalline domains can be analyzed by looking along different crystallographic directions (peaks with different Miller indices). As a novel development, pair-distribution functions which work in the real space have been applied to nanoparticles with considerable success.^[23]

Two major pitfalls should be mentioned. First, the crystallite size as determined by XRD is not the same as the particle size.^[24] In the case of twinned particles, the crystallite size will be smaller than the particle size. Only for single-crystalline particles, crystallite size and particle size are identical. Second, the instrumental peak broadening is often not considered, that is, the Scherrer equation is directly applied to the measured peak width. For broad peaks (very small domains), this error becomes increasingly smaller, but for more narrow peaks (larger domains), a considerable error is introduced if the instrumental peak broadening (which is the lower limit of a peak width) is neglected. In that case, the computed crystallite size is smaller than its actual value. **Figure 4** shows an XRD measurement that demonstrates its ability to identify core and shell of a bimetallic Au-Pd nanoparticle.^[13f,18]

4. Elemental Distribution in Bimetallic Nanoparticles

Elemental analysis on the macroscale is usually done by atomic absorption spectroscopy (AAS), by inductively coupled plasma mass spectrometry (ICP-MS), or by X-ray fluorescence analysis (XRF). In the case of bimetallic nanoparticles, it is important to assure that the elemental composition is (ideally) the same as expected by the stoichiometry of the synthesis process. It must be underscored that a thorough purification of the nanoparticles, for example, by centrifugation, filtration or dialysis, is necessary to assess the particle properties. As outlined above, not all metal ions that are present during the synthesis will be incorporated into the nanoparticles. AAS can be used after dissolution of the nanoparticles, usually accomplished by digestion in concentrated nitric acid or aqua regia (three parts HCl and one part HNO₃). Care must be taken that the digestion is complete and that no insoluble products (like AgCl) escape the analysis. For platinum metals like iridium or rhodium, a complete digestion in aqua regia is sometimes difficult unless pressure is applied. To our experience, AAS (graphite furnace) does not give the correct stoichiometry for nanoparticles unless they have been previously dissolved, although one would have expected a complete vaporization under these analytical conditions. The detection limit of AAS depends on the individual element as they all have different spectroscopic sensitivities. For the eight elements we are discussing here, the detection limits are 0.8 ppm (Ru), 2 ppm (Rh), 1.2 ppm (Pd), 0.05 ppm (Ag), 0.75 ppm (Os), 12 ppm (Ir), 24 ppm (Pt), and 1 ppm (Au). Complex environments (like

distinguished from the palladium shell (1–2 nm).^[18] Reproduced with permission.^[13d,f] Copyright 2019, Royal Society of Chemistry.

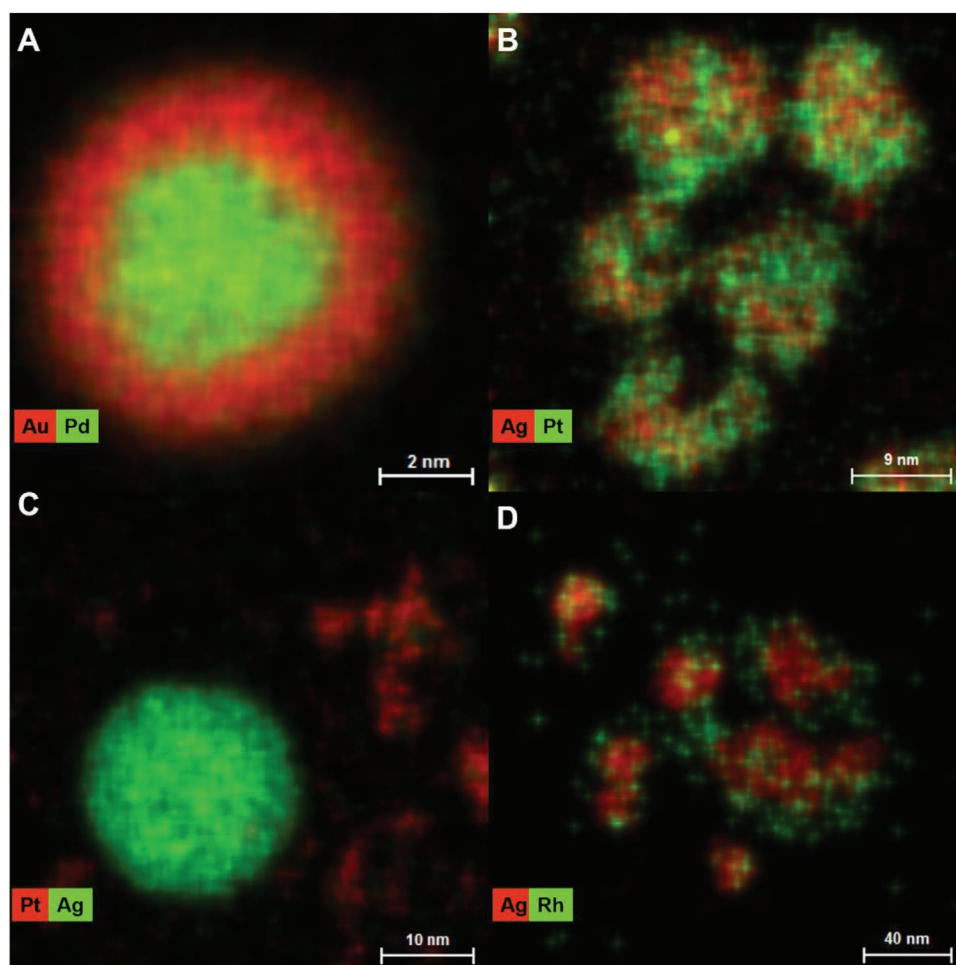


Figure 5. Elemental distribution inside typical nanoparticles: A) a palladium–gold core–shell nanoparticle, B) alloyed silver–platinum nanoparticles, C) a physical mixture of platinum and silver nanoparticles, and D) an inhomogeneous sample of partially alloyed silver–rhodium nanoparticles. Reproduced with permission.^[18,19] Copyright 2018, 2019, Kateryna Loza.

salts, biomolecules, or the presence of other metal ions) make analyses by AAS difficult and sometimes impossible.^[25] In contrast, ICP-MS is a highly sensitive method with a higher sensitivity (even below the ppt range) that can detect all elements in a sample in the same experiment.^[26] ICP-MS has also been coupled to chromatographic techniques so that an individual elemental analysis of single particles is possible.^[27] XRF works with solid samples with a detection limit of about 1 ppm. This gives reasonable data for bimetallic nanoparticles.^[28] Together with electron microscopy, energy-dispersive X-ray spectroscopy (EDX) and wavelength-dispersive X-ray spectroscopy (WDX) give semi-quantitative results for macroscopic samples. However, for accurate analytical data on nanoparticles assemblies by EDX and WDX, the samples have to be specially prepared and the instrument has to be calibrated.^[29]

For bimetallic nanoparticles, the question of the elemental distribution inside each nanoparticle becomes important.^[3b,d,f,6a,c,30] It is necessary to prove that a given population of bimetallic nanoparticles indeed contains bimetallic nanoparticles that are all identical. Particle size distributions and particle shapes cannot give this information, that is, an elemental analysis on the nanoscale is necessary. Without this information, it would be almost impossible to distinguish,

for example, a population of 10 nm Ag–Au nanoalloys from a mixture of 10 nm Ag nanoparticles and 10 nm Au nanoparticles. Thus, modern analytical techniques which can distinguish between elements on the nanometer scale and below are required. These are typically associated with high-resolution transmission electron microscopy: Energy-dispersive X-ray spectrometry (EDX) and high-angle annular dark-field imaging (HAADF).^[31] Only if the elemental distribution inside a nanoparticle is known, we can discriminate homogeneous alloy nanoparticles and core–shell nanoparticles. **Figure 5** shows representative examples of bimetallic nanoparticles with different elemental distribution.

Fundamental questions concern the distribution of the elements inside a nanoparticle (e.g., alloy or core–shell) and the crystallographic faceting (e.g., which crystal faces are exposed). For instance, it is usually not clear whether the measured elemental distribution represents a thermodynamic equilibrium state or a frozen image of the synthesis conditions. The fact that it is possible to obtain different kinds of bimetallic nanoparticles underscores the latter, that is, bimetallic nanoparticles usually represent a kinetically frozen state. Nevertheless, it is interesting to assess whether, for example, a core–shell nanoparticle will transform into a nanoalloy if sufficient energy is supplied to overcome the activation barrier for atom movement inside a

particle. This would involve heating the particles to below the sintering and melting temperature and analyze the elemental distribution before and after heating, usually by HRTEM combined with EDX or HAADF. However, it cannot be taken for granted that the equilibrium state at elevated temperature is the same as the “frozen” state after cooling to ambient temperature for individual particle analysis by HRTEM. Thus, in situ analyses at high temperature are required which are experimentally not trivial. The same considerations apply to crystal faces that may result from the specific synthetic process (e.g., influenced by capping agents) or from a stable energetic state in terms of surface energy.

It must again be stressed that the yield of a nanoparticle synthesis is not always 100%. This means that the ratio of both metals in the nanoparticles can be different from the ratio of the metallic precursors. A proper assessment requires elemental analysis of a large number of nanoparticles, that is, beyond the analysis of just a few particles by EDX and related methods. A representative amount of a sample should be analyzed by bulk methods AAS, ICP-MS, or XRF to assure the overall composition of a sample. Thus, both microscopic and macroscopic analytical methods should be used for a full characterization. Further analytical data on the elemental distribution inside nanoparticles can be obtained by X-ray absorption spectroscopy (EXAFS and XANES).^[32] and X-ray photoelectron spectroscopy (XPS).^[33]

Electrochemistry is a powerful tool to analyze metallic nanoparticles as they can all be oxidized and again reduced by application of a suitable voltage.^[34] Cyclic voltammetry (CV) is a common technique which also permits the quantitative analysis of bimetallic nanoparticles where the metals are subsequently oxidized and reduced, depending on their electrochemical potential. It is also possible to distinguish between alloyed nanoparticles and core-shell nanoparticles.^[35] The underpotential deposition, for example, of lead (Pb), permits a very sensitive surface analysis which is not possible by any other means.^[36] Another option is the single particle analysis after impact on an electrode after electrophoretic deposition in the electric field where the size of each particle can be computed from the total charge measured for each particle.^[37]

One could argue that the properties of bimetallic nanoparticles should be predictable by knowledge of the phase diagram. However, this is misleading because phase diagrams describe thermodynamic equilibrium phases.^[3f,6c] Most synthetic protocols (especially the chemical syntheses based on bottom-up approaches) involve reactions at or near ambient temperature. They also lead to kinetically stable products as it is evident from the possibility to synthesize so many different types of bimetallic nanoparticles with the same composition (alloy, core-shell, etc.). Furthermore, phase diagrams do not include surface energy effects which are important and sometimes even dominant for nanoparticles.^[3f,6c] Therefore, the knowledge of a phase diagram of a given bimetallic mixture is certainly helpful, but its predictive capacity is unfortunately limited for bimetallic nanoparticles. As an example, the system silver-platinum has a miscibility gap,^[38] but it has been shown that the synthesis of alloyed silver-platinum nanoparticles is possible.^[7a,8a,39] Electrochemical arguments have been used to predict the formation of core-shell and alloyed nanoparticles.^[40] The laser-based

synthesis of metallic nanoparticles for catalysis has also been investigated in detail as a model top-down approach.^[41]

Theoretical methods have also been applied to bimetallic nanoparticles to address these questions.^[42] Unfortunately, their predictive behavior is limited because high-end simulations can only be applied to small particles (a 1.8 nm gold nanoparticle already contains about 150 atoms) and because the influence of the organic capping agents cannot be assessed. Furthermore, most computations are carried out in vacuum which is physically correct but much different from the state of a dispersed nanoparticle. Nevertheless, the increasing computer power and refined models will probably lead to considerable advances in the future.

If nanoparticles become sufficiently small (a few nm in diameter), they are denoted as “ultrasmall.” In this dimension, they meet the size of metalloid clusters which can be considered as large molecules.^[1c,4a,43] In contrast to nanoparticles, such clusters are often atomically sharp, that is, they contain a given number of metal atoms in a defined geometric arrangement that can be probed by single-crystal X-ray diffraction.^[44] Besides a number of monometallic clusters, some bimetallic clusters have also been crystallized and structurally characterized.^[45] Such ultrasmall particles have special properties compared to larger ones, in terms of spectroscopic properties (e.g., autofluorescence instead of fluorescent quenching),^[46] biological properties (e.g., a better cell membrane permeability, also into the cell nucleus),^[47] and for heterogeneous catalysis and electrocatalysis.^[3i,48] An interesting synthetic concept is biotemplating by selective peptides to form bimetallic ultrasmall nanoparticles.^[49]

Often nanoparticles are spherical, but there is a strong interest in reliable synthetic protocols for non-spherical particles. Generally, the synthetic protocols which have been developed for monometallic nanoparticles can also be applied to bimetallic nanoparticles, that is, a successful control over nucleation and growth can lead to non-spherical nanoparticles. Seeded-growth methods are a straightforward example where a non-spherical seed of the first metal is overgrown by a shell of the second metal under retention of the particle shape.^[2b,5a,50] **Figure 6** shows representative non-spherical bimetallic nanoparticles.

There are also reports on more complicated systems that contain more than two metals. Trimetallic nanoalloys of Au-Pt-Pd have been prepared by magnetron-sputtering, and their formation has been studied by molecular dynamics simulation.^[52] The thermal behavior of trimetallic Au-Cu-Pt nanoparticles was studied by molecular dynamics to predict the melting process in such core-shell nanoparticles.^[53]

5. Optical Properties of Bimetallic Nanoparticles

Depending on the element, nanoparticles of noble metals have distinct optical properties that are different from the bulk metals.^[54] These involve surface plasmon resonance (SPR) where surface electrons are excited to give a characteristic absorption, leading to colored nanoparticle dispersions.^[55] The characteristic red color of gold nanoparticle dispersions is famous since the days of Michael Faraday, but has been used even by the Romans

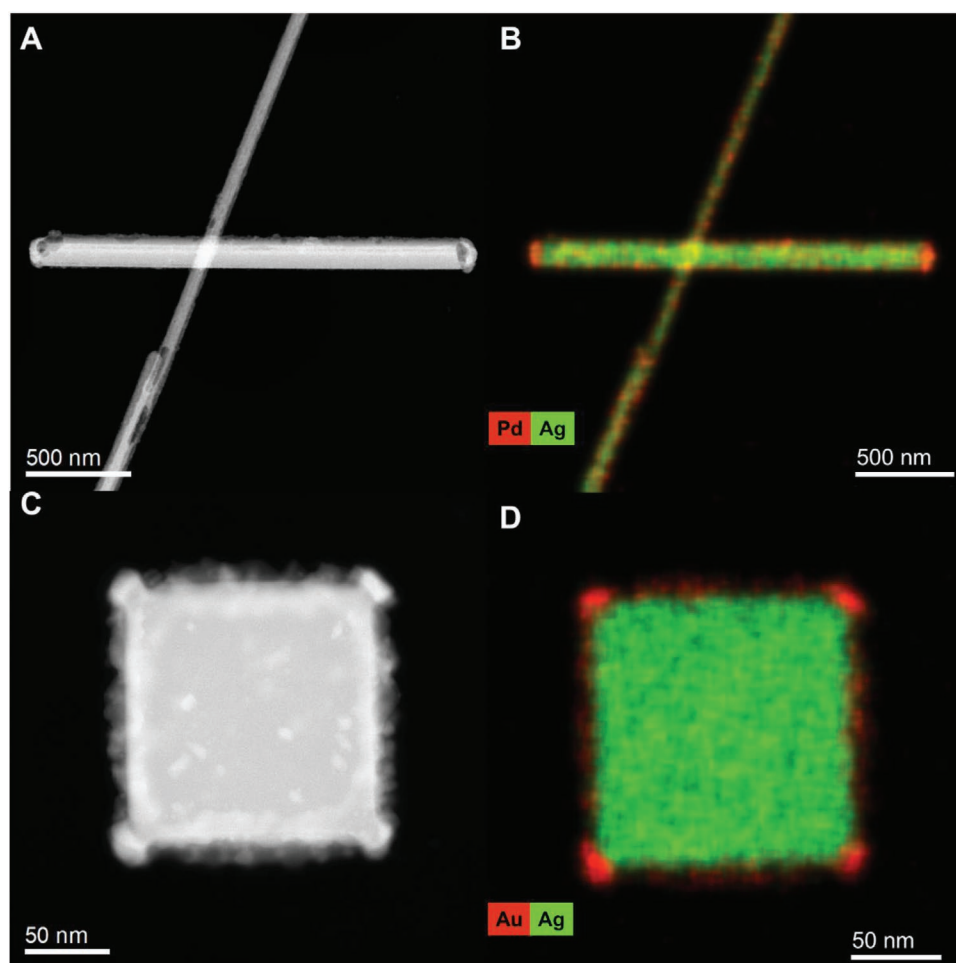


Figure 6. Representative HRTEM images of non-spherical bimetallic nanoparticles with elemental distribution by EDX. A,B) Silver nanorods, overgrown with palladium. C,D) Silver nanocubes, overgrown with gold. Reproduced with permission.^[51] Copyright 2019, Kateryna Loza.

and by medieval glassmakers to prepare colored bottles and windows.^[1e] The SPR absorption wavelength depends on the individual element. In dispersions of “common” nanoparticles of about 10–20 nm diameter, silver has a yellow color and gold has a red color. The platinum group metals do not show a distinct SPR absorption in the visible region (400–800 nm), that is, their nanoparticle dispersions are usually brownish-black colored.^[56] The wavelength and the intensity of the SPR band both depend on the particle size and the particle shape.

For bimetallic nanoparticles, the SPR can give a clue on the internal distribution of the elements. For alloyed nanoparticles, the maximum of the SPR absorption band shifts linearly with the composition. For core-shell nanoparticles, only the SPR of the metal in the shell is observed (if the shell forms a continuous layer around the core). **Figure 7** shows typical data.

Like nanoparticles, bimetallic nanoparticles have a strong capability for fluorescence quenching.^[2a,56] This makes it difficult and often impossible to attach fluorescent labels, for example, for imaging experiments in cell cultures. However, if the nanoparticles become very small (a few nm), their quenching ability is lost and an autofluorescence can result, depending on the nanoparticle and the ligand shell.^[46b,58]

6. Biological Properties of Bimetallic Nanoparticles

Two main properties of nanoparticles are important: Their uptake by cells and their potential to release bioactive ions. In general, all kinds of nanoparticles are taken up by all kinds of cells, usually by endocytosis and related mechanisms.^[59] They usually end up in the endolysosome from which they can reach the cytosol or face excretion out of the cell. Oxidation can lead to the release of metal cations, an effect that can lead to unexpected results in the case of bimetallic nanoparticles. When two metals with different electrode potential are electrically coupled, a local element results which can lead to a preferential oxidation of the less noble metal. This effect is important for silver which is the most bioactive of the eight metals discussed here. Silver has a well-known cytotoxic effect toward bacteria and cells which is frequently exploited for antibacterial coatings.^[1b,60] In contrast, the other noble metals form nanoparticles which are much less cytotoxic and often have small biological effects, if at all.^[61] In silver-alloyed nanoparticles, the release of silver can lead to a tunable cytotoxicity, but experience has shown that it is difficult to predict the exact level of cytotoxicity.^[39f,60a,62] The

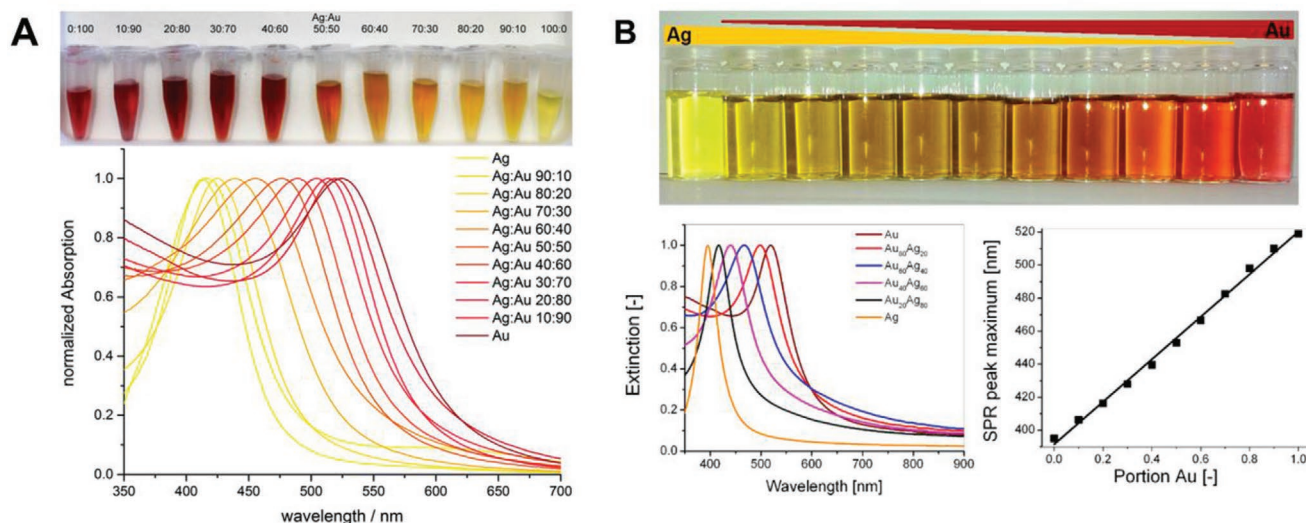


Figure 7. Optical properties of bimetallic nanoparticles: Alloyed silver–gold nanoparticles prepared by A) wet-chemical reduction and by B) laser ablation. It is remarkable that bimetallic nanoparticles from these very different synthetic approaches show such similar optical properties. A) Reproduced with permission.^[16,22a] Copyright 2015, Royal Society of Chemistry. B) Reproduced under the terms and conditions of the Creative Commons Attribution License.^[9d] Copyright 2014, The Authors, published by Beilstein-Institut.

presence of platinum in alloyed silver–platinum nanoparticles causes an osteopromotive activity in contact with human mesenchymal stem cells.^[63] **Figure 8** shows typical cell-biological data of bimetallic nanoparticles.

Due to its antibacterial action, bimetallic nanoparticles that contain silver are most prominent in biomedical applications.^[64] This was also shown for a range of bimetallic silver-containing surface coatings, deposited by magnetron sputtering.^[65] However, the exact reasons and mechanisms of the observed biological effects often remain unclear and require a laborious investigation of materials scientists together with biologists. It must be stressed that bimetallic nanoparticles can strongly differ in their properties as outlined above, that is, an assessment of the biological effect must be accompanied by a thorough analysis of the nanoparticle structure itself, mainly the elemental distribution inside the nanoparticles. It is not sufficient to use the average particle size and the overall elemental composition to predict the biological effect of bimetallic nanoparticles.

In terms of regulatory affairs, the framework laid out by organizations like the U.S. American Federal Drug Administration (FDA) and the European Union (EU) are important. Typically, nanomaterials are defined by one or more characteristic dimensions between 1 and 100 nm.^[66] Both FDA and EU are regulating the application in consumer products, in biomedical devices, and in drugs. Thus, if a bimetallic nanoparticle falls into this size range, it will be considered as a nanomaterial. To assess the biological effects and potential risks, all properties that are discussed above (e.g., size, average size distribution, shape, charge, surface functionalization) have to be considered. For a bimetallic nanoparticle, the inner structure, that is, mainly the elemental distribution, and the elemental composition (ratio of metals) need to be provided as further parameters because they will affect the biological properties. It is probably not an exaggeration to assume that the approval process for a bimetallic nanoparticle system for biomedical application will be a regulatory nightmare.

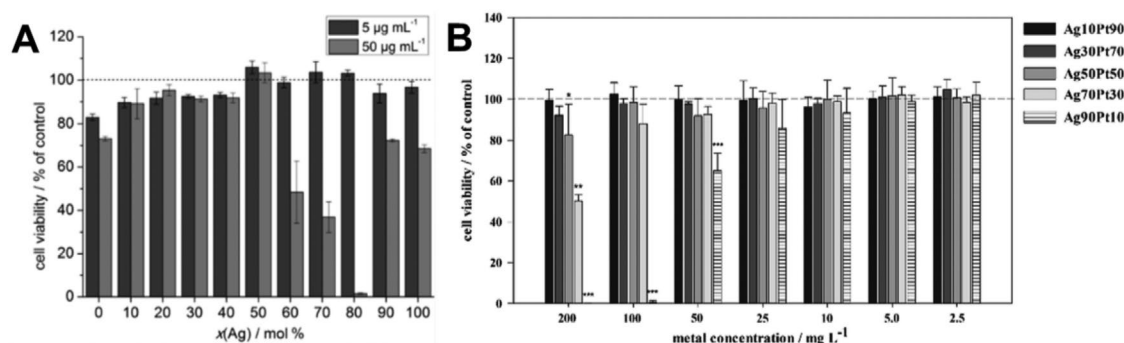


Figure 8. A) Effect of silver–gold nanoparticles on the viability of human mesenchymal stem cells. B) Effect of silver–platinum nanoparticles on the viability of human mesenchymal stem cells. Reproduced under the terms and conditions of the Creative Commons Attribution License.^[62c] Copyright 2015, The Authors, published by Beilstein-Institut. B) Reproduced with permission.^[39f] Copyright 2018, Royal Society of Chemistry.

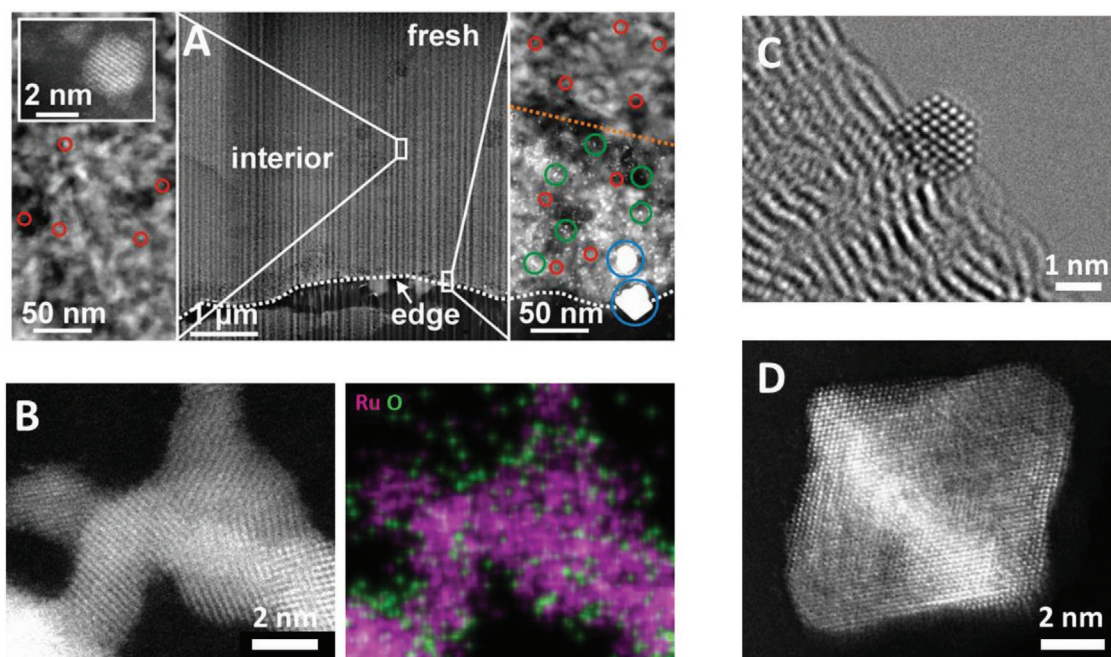


Figure 9. A) STEM images of a Pt-Pd/Al₂O₃ CO oxidation catalyst. The left and right columns show magnified images of the interior and outer edge of the alumina support, respectively. Colored circles indicate different-sized Pt-Pd nanoparticles. Reproduced with permission.^[71] Copyright 2017, Wiley-VCH. B) STEM image and EDX map of Ru/RuO₂ OER catalyst clusters. Reproduced with permission.^[72] Copyright 2018, American Chemical Society. C) HRTEM image of a platinum fuel cell catalyst nanoparticle on a carbon substrate. D) STEM image of a faceted platinum–nickel alloy catalyst. Reproduced with permission. Copyright 2019, Marc Heggen.

7. Application of Bimetallic Nanoparticles in Heterogeneous Catalysis

Heterogeneous catalysis strongly relies on metals, usually in finely dispersed form to enhance the catalytically active specific surface area.^[3d,67] A plethora of supported metal catalysts has been described, explored, and brought to practical application. The application of bimetallic nanoparticles broadens the range of heterogeneous catalysis, for example, for fine-tuning the redox activity in alloyed nanoparticles in redox catalysis and electrocatalysis.^[2d,3g,h,i,j,k,54,68] Noble metal nanoparticles are important electrocatalysts, for example, in polymer electrolyte membrane (PEM) water electrolysis and fuel cells. Ruthenium (Ru/RuO₂) and iridium (Ir/IrO₂) are the most active catalysts for the oxygen evolution reaction (OER) at the anode in water electrolysis. Ruthenium is more active than iridium, but as corrosion limits the use of ruthenium, iridium is generally considered as the state-of-the-art catalyst for the OER in PEM water electrolysis.^[69] The reference catalyst for the hydrogen evolution reaction (HER) at the cathode in PEM water electrolysis is platinum. In addition, platinum nanoparticles are also benchmark catalysts for the hydrogen oxidation reaction (HOR) as well for the oxygen reduction reaction (ORR) in PEM fuel cells (**Figure 9**). Especially the ORR requires a high platinum loading due to its sluggish kinetics.^[70]

It should be noted that the activity of noble metal catalysts, for instance, for the ORR can be substantially increased by alloying them with more abundant transition metals like nickel. Such alloying strategies can be used to introduce lattice compression effects^[73] and/or to modify the electronic properties.^[74] Furthermore, the selection of highly active facets and

the use of faceted nanoparticles can substantially increase the catalytic activity. For instance, it has been demonstrated that the Pt₃Ni (111) alloy surface has an exceptionally high ORR activity (**Figure 9**).^[75] It is ten times more active than the platinum (111) surface and 90 times more active than state-of-the-art spherical platinum catalysts. In addition, surface doping with a ternary metal is a highly effective strategy to stabilize the octahedral shapes of the catalyst nanoparticles and to improve their long-term stability during electrochemical cycling.^[76] As palladium has similar properties as platinum but is less costly, it is sometimes considered as a substitute for platinum catalysts. Thus, palladium was tested in fuel cells as platinum co-catalyst as anode and cathode material in acid media and as anode material in alkaline membrane fuel cell.^[77]

For the storage of hydrogen produced by sustainable resources, ammonia has been suggested due to its high energy density compared to hydrogen. Ruthenium-based catalysts have the highest activity for the decomposition of ammonia into hydrogen and nitrogen.^[78] As further examples for noble metals in gas-phase catalysis, palladium and palladium/silver are state-of-the-art catalysts for the semi-hydrogenation of acetylene, which is an industrially important reaction for the purification of an ethylene feed for the production of polyethylene.^[79] Supported noble metal catalysts like platinum, palladium, and gold are also used to oxidize volatile organic compounds.^[80] Gold is a highly effective catalyst for the oxidation of CO at very low temperatures. Because of this, gold has also been used as catalyst for the water gas shift reaction (CO + H₂O → CO₂ + H₂), a reaction which is crucial for the production of hydrogen on an industrial scale.^[81] Gold and silver are also active catalysts for the electrochemical reduction of CO₂. Furthermore, platinum,

palladium, and rhodium are used as automotive exhaust catalysts, where platinum and palladium serve as oxidation catalysts (Figure 9) and rhodium and platinum serve as reduction catalysts. Thus, bimetallic nanoparticles of noble metals offer many opportunities that go beyond the individual metals or their physical mixtures.

The performance of bimetallic nanoparticles and metal alloy surfaces in heterogeneous catalysis has been studied by theoretical methods. Only a few examples can be discussed here. Electronic effects were shown by density-functional theory (DFT) to control the adsorption of oxygen and its dissociation on the surface on Ag-Au alloys.^[82] A synergetic effect of palladium and gold was found by DFT for formic acid decomposition to enhance the hydrogen production rate.^[83] The melting of Au-Pd nanoalloys was predicted by molecular dynamics simulations.^[84] A DFT analysis in the Pd-Ir system was performed to describe the hydrogen-metal interaction which was weakened by the presence of iridium.^[85] The influence of the particle structure and internal elemental distribution was approached both experimentally and theoretically (by DFT simulations) on Pt-Au nanoparticles (7 nm), and compositions with a maximum catalytic efficiency were identified on the basis of the surface atom arrangement.^[86] The strain inside nanoparticles was decisive for the catalytic performance in electrocatalysis.^[68c] By DFT calculations, an optimized composition of RhAu nanoparticles was predicted that was efficient in the oxygen-reduction reaction. Notably, rhodium and gold are immiscible in the bulk state and can only be alloyed as nanoparticle.^[87] It has also been argued, based on extensive DFT simulations, that the catalytic effects on nanoparticles cannot be easily compared to model surfaces that are, however, more easily defined.^[68a]

8. Conclusions and Future Developments

A considerable amount of work has been reported for bimetallic nanoparticles. On summary, they extend the field of potential applications beyond monometallic nanoparticles. Based on the current state-of-the-art, we envision future developments in the following directions.

First, it will be interesting to blend three or more metals in one nanoparticle. This touches the field of high-entropy alloys in materials science. The synthesis and the structural characterization will be more complex, but a possible fine-tuning of the properties could give rise to new applications, for example, in heterogeneous catalysis. However, an empirical understanding of the synthetic procedures and the observed effects will be increasingly difficult, given the many degrees of freedom for such complex nanoparticles.

Second, there is the perspective to make the bimetallic nanoparticles smaller until they reach the size of ultrasmall particles which meet the area of atom-sharp clusters. In this case, the particle diameters are at about 2 nm and below. From such particles, novel applications (e.g., imaging in cell biology) and a better cell wall permeation can be expected.

Third, ultrastructural methods will gain further importance to bring our knowledge of the internal crystallography and the elemental distribution inside individual nanoparticles to a higher level. For instance, high-resolution electron microscopy,

also applied in situ, and atom probe tomography (APT) should be able to shed light onto the structure on the level of individual atoms. The results will also go into the third dimension, that is, electron tomographic techniques will be combined with spectroscopic techniques with atomic resolution (EDX, HAADF). At the moment, we can identify elements inside a particle, but the detection of a possible enrichment or depletion along dislocation steps is still beyond our experimental abilities. Electrochemistry and single-particle analyses will strongly contribute to our knowledge.

Fourth, synthetic approaches will be accompanied by in situ methods where we will learn more on the particle formation processes of bimetallic nanoparticles, for example, small-angle X-ray scattering (SAXS), small-angle neutron scattering (SANS), X-ray absorption spectroscopy (XANES, EXAFS)

Fifth, theoretical method will permit us to predict and understand properties of bimetallic nanoparticles as computers are becoming faster and relevant systems become larger. This will help us to develop and to improve more reliable and robust synthetic pathways, both bottom-up and top-down, also to produce bimetallic nanoparticles in larger amounts.

Acknowledgements

The authors thank the Deutsche Forschungsgemeinschaft (DFG) for funding within the projects EP 22/44-1, HE 7192/2-1, HE 7192/1-1, and HE 7192/1-2. They thank Dr. Viktoria Grasmik, Dr. Kevin Pappert, Dr. Simon Ristig, and Dr. Alexander Rostek for material from their publications and Ph.D. theses.

Conflict of Interest

The authors declare no conflict of interest.

Keywords

alloys, antibacterial properties, heterogeneous catalysis, nanoparticles, noble metals

Received: November 6, 2019

Revised: December 13, 2019

Published online: March 5, 2020

- [1] a) D. Pedone, M. Moglianetti, E. De Luca, G. Bardi, P. P. Pompa, *Chem. Soc. Rev.* **2017**, 46, 4951; b) S. Chernousova, M. Eppe, *Angew. Chem., Int. Ed.* **2013**, 52, 1636; c) L. Dykman, N. Khlebtsov, *Chem. Soc. Rev.* **2012**, 41, 2256; d) M. Homberger, U. Simon, *Phil. Trans. R. Soc. A* **2010**, 368, 1405; e) H. Goesmann, C. Feldmann, *Angew. Chem., Int. Ed.* **2010**, 49, 1362; f) R. A. Sperling, P. Rivera, F. Zhang, M. Zanella, W. J. Parak, *Chem. Soc. Rev.* **2008**, 37, 1896; g) J. J. Giner-Casares, M. Henriksen-Lacey, M. Coronado-Puchau, L. M. Liz-Marzán, *Mater. Today* **2016**, 19, 19.
- [2] a) R. Yu, L. M. Liz-Marzán, F. J. García de Abajo, *Chem. Soc. Rev.* **2017**, 46, 6710; b) Y. Xia, X. Xia, Y. Wang, S. Xie, *MRS Bull.* **2013**, 38, 335; c) J. Zeng, Y. Zheng, M. Rycenga, J. Tao, Z. Y. Li, Q. Zhang, Y. Zhu, Y. N. Xia, *J. Am. Chem. Soc.* **2010**, 132, 8552; d) S. Zhou, M. Zhao, T. H. Yang, Y. N. Xia, *Mater. Today* **2019**, 22, 108.

- [3] a) D. Zhang, B. Gökce, S. Barcikowski, *Chem. Rev.* **2017**, *117*, 3990; b) L. Zhang, Z. Xie, J. Gong, *Chem. Soc. Rev.* **2016**, *45*, 3916; c) Y. Xu, L. Chen, X. Wang, W. Yao, Q. Zhang, *Nanoscale* **2015**, *7*, 10559; d) H. L. Liu, F. Nosheen, X. Wang, *Chem. Soc. Rev.* **2015**, *44*, 3056; e) M. B. Cortie, A. M. McDonagh, *Chem. Rev.* **2011**, *111*, 3713; f) R. Ferrando, J. Jellinek, R. L. Johnston, *Chem. Rev.* **2008**, *108*, 845; g) H. Mistry, A. S. Varela, S. Kuhl, P. Strasser, B. R. Cuenya, *Nat. Rev. Mater.* **2016**, *1*, 16009; h) C. Z. Zhu, D. Du, A. Eychmüller, Y. H. Lin, *Chem. Rev.* **2015**, *115*, 8896; i) J. B. Zhao, R. C. Jin, *Nano Today* **2018**, *18*, 86; j) G. F. Liao, J. S. Fang, Q. Li, S. H. Li, Z. S. Xu, B. Z. Fang, *Nanoscale* **2019**, *11*, 7062; k) J. Gu, Y. W. Zhang, F. Tao, *Chem. Soc. Rev.* **2012**, *41*, 8050.
- [4] a) K. Zarschler, L. Rocks, N. Licciardello, L. Boselli, E. Polo, K. P. Garcia, L. De Cola, H. Stephan, K. A. Dawson, *Nanomedicine* **2016**, *12*, 1663; b) W. J. Stark, P. R. Stoessel, W. Wohlleben, A. Hafner, *Chem. Soc. Rev.* **2015**, *44*, 5793; c) C. M. Cobley, J. Y. Chen, E. C. Cho, L. V. Wang, Y. N. Xia, *Chem. Soc. Rev.* **2011**, *40*, 44; d) P. Wagener, J. Jakobi, C. Rehbock, V. S. K. Chakravadhanula, C. Thede, U. Wiedwald, M. Bartsch, L. Kienle, S. Barcikowski, *Sci. Rep.* **2016**, *6*, 23352.
- [5] a) Y. Xia, K. D. Gilroy, H. Peng, C. X. Xia, *Angew. Chem.* **2017**, *129*, 60; b) T. Xia, M. Kovochich, M. Liong, H. Meng, S. Kabehie, S. George, J. I. Zink, A. E. Nel, *ACS Nano* **2009**, *10*, 3273.
- [6] a) G. Guisbiers, R. Mendoza-Cruz, L. Bazan-Diaz, J. J. Velazquez-Salazar, R. Mendoza-Perez, J. A. Robledo-Torres, J. L. Rodriguez-Lopez, J. M. Montejano-Carrizales, R. L. Whetten, M. Jose-Yacamán, *ACS Nano* **2016**, *10*, 188; b) K. McNamara, S. A. Tofail, *Phys. Chem. Chem. Phys.* **2015**, *17*, 27981; c) F. Calvo, *Phys. Chem. Chem. Phys.* **2015**, *17*, 27922; d) M. Sankar, N. Dimitratos, P. J. Miedziak, P. P. Wells, C. J. Kiely, G. J. Hutchings, *Chem. Soc. Rev.* **2012**, *41*, 8099.
- [7] a) S. Krishnan, M. Estevez-González, R. Perez, R. Esparza, M. Meyyappan, *RSC Adv.* **2017**, *7*, 27170; b) Y. G. Sun, Y. N. Xia, *Science* **2002**, *298*, 2176; c) C. M. Cobley, M. Rycenga, F. Zhou, Z. Y. Li, Y. N. Xia, *Angew. Chem., Int. Ed.* **2009**, *48*, 4824.
- [8] a) T. Fu, J. Fang, C. Wang, J. Zhao, *J. Mater. Chem. A* **2016**, *4*, 8803; b) C. Bock, C. Paquet, M. Couillard, G. A. Botton, B. R. MacDougall, *J. Am. Chem. Soc.* **2004**, *126*, 8028; c) F. Papa, C. Negri, A. Miyazaki, I. Balint, *J. Nanopart. Res.* **2011**, *13*, 5057.
- [9] a) I. Lee, S. W. Han, K. Kim, *Chem. Commun.* **2001**, 1782; b) D. Tiedemann, U. Taylor, C. Rehbock, J. Jakobi, S. Klein, W. A. Kues, S. Barcikowski, D. Rath, *Analyst* **2014**, *139*, 931; c) A. Neumeister, J. Jakobi, C. Rehbock, J. Moysig, S. Barcikowski, *Phys. Chem. Chem. Phys.* **2014**, *16*, 23671; d) C. Rehbock, J. Jakobi, L. Gamrad, S. van der Meer, D. Tiedemann, U. Taylor, W. A. Kues, D. Rath, S. Barcikowski, *Beilstein J. Nanotechnol.* **2014**, *5*, 1523; e) G. K. Podagatlapalli, S. H. Hamad, S. V. Rao, *J. Phys. Chem. C* **2015**, *119*, 16972.
- [10] a) Y. H. Chen, C. S. Yeh, *Chem. Commun.* **2001**, 371; b) S. Besner, M. Meunier, *J. Phys. Chem. C* **2010**, *114*, 10403; c) R. Intartaglia, G. Das, K. Bagga, A. Gopalakrishnan, A. Genovese, M. Povia, E. Di Fabrizio, R. Cingolani, A. Diaspro, F. Brandi, *Phys. Chem. Chem. Phys.* **2013**, *15*, 3075.
- [11] a) Y. Dieckmann, H. Colfen, H. Hofmann, A. Petri-Fink, *Anal. Chem.* **2009**, *81*, 3889; b) D. Mahl, J. Diendorf, W. Meyer-Zaika, M. Eppe, *Coll. Surf. A* **2011**, *377*, 386; c) H. Fissan, S. Ristig, H. Kaminski, C. Asbach, M. Eppe, *Anal. Meth.* **2014**, *6*, 7324; d) A. Letzel, B. Gökce, A. Menzel, A. Plech, S. Barcikowski, *Appl. Surf. Sci.* **2018**, *435*, 743; e) Y. J. Song, Z. S. Zhang, H. E. Elsayed-Ali, H. N. Wang, L. L. Henry, Q. Q. Wang, S. L. Zou, T. Zhang, *Nanoscale* **2011**, *3*, 31.
- [12] H. Lange, *Part. Part. Syst. Charact.* **1995**, *12*, 148.
- [13] a) X. L. Chen, J. Schroder, S. Hauschild, S. Rosenfeldt, M. Dulle, S. Forster, *Langmuir* **2015**, *31*, 11678; b) S. Yan, Z. H. Wu, H. Y. Yu, Y. Gong, Y. Y. Tan, R. Du, W. Chen, X. Q. Xing, G. Mo, Z. J. Chen, Q. Cai, D. B. Sun, *J. Phys. Chem. C* **2014**, *118*, 11454; c) J. Polte, T. T. Ahner, F. Delissen, S. Sokolov, F. Emmerling, A. F. Thünemann, R. Kraehnert, *J. Am. Chem. Soc.* **2010**, *132*, 1296; d) A. Rostek, M. Breisch, K. Loza, P. R. A. F. Garcia, C. L. P. Oliveira, O. Prymak, M. Heggen, M. Köller, C. Sengstock, M. Eppe, *ChemistrySelect* **2018**, *3*, 4994; e) P. R. A. F. Garcia, K. Loza, S. Daumann, V. Grasmik, K. Pappert, A. Rostek, J. Helmlinger, O. Prymak, M. Heggen, M. Eppe, C. L. P. Oliveira, *Braz. J. Phys.* **2019**, *49*, 183; f) A. Rostek, K. Loza, M. Heggen, M. Eppe, *RSC Adv.* **2019**, *9*, 26628.
- [14] a) J. Baumgard, M. M. Pohl, U. Kragl, N. Steinfeldt, *Nanotechnol. Rev.* **2014**, *3*, 87; b) H. Hagendorfer, R. Kaegi, M. Parlinska, B. Sinnet, C. Ludwig, A. Ulrich, *Anal. Chem.* **2012**, *84*, 2678; c) M. Lattuada, C. Olivo, C. Gauer, G. Storti, M. Morbidelli, *Langmuir* **2010**, *26*, 7062.
- [15] J. L. Brennan, N. S. Hatzakis, T. R. Tshikhudo, V. Razumas, S. Patkar, J. Vind, A. Svendsen, R. J. M. Nolte, A. E. Rowan, M. Brust, *Bioconjugate Chem.* **2006**, *17*, 1373.
- [16] S. Ristig, *Ph.D. Thesis*, University of Duisburg-Essen **2014**.
- [17] S. Banerjee, K. Loza, W. Meyer-Zaika, O. Prymak, M. Eppe, *Chem. Mater.* **2014**, *26*, 951.
- [18] A. Rostek, *Ph.D. Thesis*, University of Duisburg-Essen **2019**.
- [19] V. Grasmik, *Ph.D. Thesis*, University of Duisburg-Essen **2018**.
- [20] a) S. J. L. Billinge, I. Levin, *Science* **2007**, *316*, 561; b) D. Jose, B. R. Jagirdar, *J. Phys. Chem. C* **2008**, *112*, 10089; c) O. V. Belousov, N. V. Belousova, A. V. Sirotina, L. A. Solov'yov, A. M. Zhyzhayev, S. M. Zharkov, Y. L. Mikhlin, *Langmuir* **2011**, *27*, 11697; d) C. Weidenthaler, *Nanoscale* **2011**, *3*, 792.
- [21] a) O. Prymak, J. Jakobi, C. Rehbock, M. Eppe, S. Barcikowski, *Mater. Chem. Phys.* **2018**, *207*, 442; b) S. Xiong, H. Ozturk, S. Y. Lee, P. M. Mooney, I. C. Noyan, *J. Appl. Cryst.* **2018**, *51*, 1102.
- [22] a) S. Ristig, O. Prymak, K. Loza, M. Gocyla, W. Meyer-Zaika, M. Heggen, D. Raabe, M. Eppe, *J. Mater. Chem. B* **2015**, *3*, 4654; b) C. Solliard, M. Flueli, *Surf. Sci.* **1985**, *156*, 487; c) M. Y. Gamarnik, Y. Y. Sidorin, *Phys. Stat. Sol. B* **1989**, *156*, K1; d) V. Petkov, S. Shastri, S. Shan, P. Joseph, J. Luo, C. J. Zhong, T. Nakamura, Y. Herban, S. Sato, *J. Phys. Chem. C* **2013**, *117*, 22131; e) A. V. Girao, P. C. Pinheiro, M. Ferro, T. Trindade, *RSC Adv.* **2017**, *7*, 15944; f) G. Bozzolo, J. E. Garcés, G. N. Derry, *Surf. Sci.* **2007**, *601*, 2038.
- [23] a) S. Banerjee, C. H. Liu, J. D. Lee, A. Kovyakh, V. Grasmik, O. Prymak, C. Koenigsmann, H. Liu, L. Wang, A. M. M. Abeykoon, S. S. Wong, M. Eppe, C. B. Murray, S. J. L. Billinge, *J. Phys. Chem. C* **2018**, *122*, 29498; b) M. Zobel, R. B. Neder, S. A. J. Kimber, *Science* **2015**, *347*, 292; c) K. M. O. Jensen, P. Juhas, M. A. Tofanelli, C. L. Heinecke, G. Vaughan, C. J. Ackerson, S. J. L. Billinge, *Nat. Comm.* **2016**, *7*, 11859.
- [24] H. P. Klug, L. E. Alexander, *X-ray Diffraction Procedures for Polycrystalline and Amorphous Materials*, Wiley-Interscience, New York, **1974**.
- [25] K. Loza, M. Eppe, *RSC Adv.* **2018**, *8*, 24386.
- [26] a) D. G. Thomas, J. N. Smith, B. D. Thrall, D. R. Baer, H. Jolley, P. Munusamy, V. Kodali, P. Demokritou, J. Cohen, J. G. Teeguarden, *Part. Fibre Toxicol.* **2018**, *15*, 22; b) M. Sikder, J. R. Lead, G. T. Chandler, M. Baalousha, *Sci. Total Environ.* **2018**, *618*, 597; c) J. P. Kaiser, M. Roesslein, L. Diener, A. Wichser, B. Nowack, P. Wick, *J. Nanobiotechnol.* **2017**, *15*, 11.
- [27] a) Z. Q. Tan, Y. G. Yin, X. R. Guo, M. Amde, M. H. Moon, J. F. Liu, G. B. Jiang, *Environ. Sci. Technol.* **2017**, *51*, 12369; b) C. K. Su, Y. C. Sun, *J. Anal. At. Spectrom.* **2015**, *30*, 1689; c) U. Hansen, A. F. Thuenemann, *Langmuir* **2015**, *31*, 6842.
- [28] S. Suzuki, T. Suzuki, Y. Tomita, M. Hirano, K. I. Okazaki, S. Kuwabata, T. Torimoto, *CrystEngComm* **2012**, *14*, 4922.
- [29] D. E. Newbury, N. W. M. Ritchie, *Scanning* **2013**, *35*, 141.
- [30] L. Wei, W. Qi, B. Huang, M. Wang, *Comput. Mater. Sci.* **2013**, *69*, 374.

- [31] M. Alania, T. Altantzis, A. de Backer, I. Lobato, S. Bals, S. van Aert, *Ultramicroscopy* **2017**, 177, 36.
- [32] a) C. Antoniaki, *Beilstein J. Nanotechnol.* **2011**, 2, 237; b) C. A. Rodríguez-Proenza, J. P. Palomares-Báez, M. A. Chávez-Rojas, A. F. García-Ruiz, C. L. Azanza-Ricardo, A. Santoveña-Urbe, G. Luna-Bárcenas, J. L. Rodríguez-López, R. Esparza, *Materials* **2018**, 11, 1882; c) J. Timoshenko, C. J. Wrasman, M. Luneau, T. Shirman, M. Cargnello, S. R. Bare, J. Aizenberg, C. M. Friend, A. I. Frenkel, *Nano Lett.* **2018**, 19, 520.
- [33] L. Soler, A. Casanovas, J. Ryan, I. Angurell, C. Escudero, V. Pérez-Dieste, J. Llorca, *ACS Catal.* **2019**, 9, 3641.
- [34] a) K. Tschulik, K. Ngamchuea, C. Ziegler, M. G. Beier, C. Damm, A. Eychmueller, R. G. Compton, *Adv. Funct. Mater.* **2015**, 25, 5149; b) E. N. Saw, V. Grasmik, C. Rurainsky, M. Eppe, K. Tschulik, *Faraday Discuss.* **2016**, 193, 327; c) B. J. Plowman, B. Sidhureddy, S. V. Sokolov, N. P. Young, A. Chen, R. G. Compton, *ChemElectroChem* **2016**, 3, 1039.
- [35] V. Grasmik, C. Rurainsky, K. Loza, M. V. Evers, O. Prymak, M. Heggen, K. Tschulik, M. Eppe, *Chem. - Eur. J.* **2018**, 24, 9051.
- [36] a) J. Solla-Gullon, P. Rodriguez, E. Herrero, A. Aldaz, J. M. Feliu, *Phys. Chem. Chem. Phys.* **2008**, 10, 1359; b) Y. Wang, E. Laborda, C. Salter, A. Crossley, R. G. Compton, *Analyst* **2012**, 137, 4693; c) M. Kamundi, L. Bromberg, E. Fey, C. Mitchell, M. Fayette, N. Dimitrov, *J. Phys. Chem. C* **2012**, 116, 14123; d) C. Jayabharathi, M. Zander, F. Scholz, *J. Electroanal. Chem.* **2018**, 819, 159.
- [37] a) I. R. Holt, B. J. Plowman, N. P. Young, K. Tschulik, R. G. Compton, *Angew. Chem., Int. Ed.* **2016**, 55, 397; b) K. J. Stevenson, K. Tschulik, *Curr. Opin. Electrochem.* **2017**, 6, 38.
- [38] a) P. Durussel, P. Feschotte, *J. Alloys Compd.* **1996**, 239, 226; b) I. Karakaya, W. T. Thompson, *Bull. Alloy Phase Diagrams* **1988**, 9, 334.
- [39] a) J. Gao, X. Ren, D. Chen, F. Tang, J. Ren, *Scr. Mater.* **2007**, 57, 687; b) Z. Peng, H. Yang, *J. Solid State Chem.* **2008**, 181, 1546; c) K. Torigoe, Y. Nakajima, K. Esumi, *J. Phys. Chem.* **1993**, 97, 8304; d) M. L. Wu, L. B. Lai, *Colloids Surf., A* **2004**, 244, 149; e) S. Chen, S. Thota, X. Wang, J. Zhao, *J. Mater. Chem. A* **2016**, 4, 9038; f) V. Grasmik, M. Breisch, K. Loza, M. Heggen, M. Köller, C. Sengstock, M. Eppe, *RSC Adv.* **2018**, 8, 38582.
- [40] C. Tojo, D. Buceta, M. A. Lopez-Quintela, *Catalysts* **2017**, 7, 17.
- [41] S. Reichenberger, G. Marzun, M. Muhler, S. Barcikowski, *ChemCatChem* **2019**, 11, 4489.
- [42] a) S. Divi, A. Chatterjee, *RSC Adv.* **2018**, 8, 10409; b) F. Monji, M. A. Jabbareh, *CALPHAD: Comput. Coupling Phase Diagrams Thermochem.* **2017**, 58, 1; c) M. J. Cui, H. M. Lu, H. P. Jiang, Z. H. Cao, X. K. Meng, *Sci. Rep.* **2017**, 7, 10.
- [43] a) G. Schmid, W. G. Kreyling, U. Simon, *Arch. Toxicol.* **2017**, 91, 3011; b) R. Mathaes, G. Winter, A. Besheer, J. Engert, *Expert Opin. Drug Delivery* **2015**, 12, 481; c) A. Leifert, Y. Pan-Bartnek, U. Simon, W. Jahnke-Dechent, *Nanoscale* **2013**, 5, 6224; d) Y. C. Yeh, B. Creran, V. M. Rotello, *Nanoscale* **2012**, 4, 1871; e) Y. Lu, W. Chen, *Chem. Soc. Rev.* **2012**, 41, 3594; f) E. C. Dreaden, A. M. Alkilany, X. Huang, C. J. Murphy, M. A. El-Sayed, *Chem. Soc. Rev.* **2012**, 41, 2740; g) L. Shang, S. J. Dong, G. U. Nienhaus, *Nano Today* **2011**, 6, 401; h) K. Y. Zheng, X. Yuan, N. Goswami, Q. B. Zhang, J. P. Xie, *RSC Adv.* **2014**, 4, 60581; i) C. J. Zeng, *Pure Appl. Chem.* **2018**, 90, 1409; j) L. A. Dykman, N. G. Khlebtsov, *Biomaterials* **2016**, 108, 13; k) T. Ruks, C. Beuck, T. Schaller, F. Niemeyer, M. Zähres, K. Loza, M. Heggen, U. Hagemann, C. Mayer, P. Bayer, M. Eppe, *Langmuir* **2019**, 35, 767.
- [44] a) P. D. Jadzinsky, G. Calero, C. J. Ackerson, D. A. Bushnell, R. D. Kornberg, *Science* **2007**, 318, 430; b) L. Xiong, S. Yang, X. S. Sun, J. S. Chai, B. Rao, L. H. Yi, M. Z. Zhu, Y. Pei, *J. Phys. Chem. C* **2018**, 122, 14898; c) S. Kenzler, C. Schrenk, A. R. Frojd, H. Hakkinen, A. Z. Clayborne, A. Schnepf, *Chem. Commun.* **2018**, 54, 248; d) Z. Lei, J. J. Li, X. K. Wan, W. H. Zhang, Q. M. Wang, *Angew. Chem., Int. Ed.* **2018**, 57, 8639; e) N. A. Sakthivel, A. Dass, *Acc. Chem. Res.* **2018**, 51, 1774; f) Q. Yao, X. Yuan, V. Fung, Y. Yu, D. T. Leong, D. Jiang, J. Xie, *Nat. Commun.* **2017**, 8, 927; g) T. R. Tero, S. Malola, B. Koncz, E. Pohjolainen, S. Lautala, S. Mustalahti, P. Permi, G. Groenhof, M. Pettersson, H. Hakkinen, *ACS Nano* **2017**, 11, 11872.
- [45] J. Z. Yan, S. Malola, C. Y. Hu, J. Peng, B. Dittrich, B. K. Teo, H. Hakkinen, L. S. Zheng, N. F. Zheng, *Nat. Commun.* **2018**, 9, 3357.
- [46] a) S. Ristig, D. Kozlova, W. Meyer-Zaika, M. Eppe, *J. Mater. Chem. B* **2014**, 2, 7887; b) L. Shang, F. Stockmar, N. Azadfar, G. U. Nienhaus, *Angew. Chem., Int. Ed.* **2013**, 52, 11154.
- [47] a) S. B. van der Meer, K. Loza, K. Wey, M. Heggen, C. Beuck, P. Bayer, M. Eppe, *Langmuir* **2019**, 35, 7191; b) S. Huo, S. Jin, X. Ma, X. Xue, K. Yang, A. Kumar, P. C. Wang, J. Zhang, Z. Hu, X. J. Liang, *ACS Nano* **2014**, 8, 5852.
- [48] K. Kwak, W. Choi, Q. Tang, M. Kim, Y. Lee, D. E. Jiang, D. Lee, *Nat. Commun.* **2017**, 8, 14723.
- [49] N. M. Bedford, A. R. Showalter, T. J. Woehl, Z. E. Hughes, S. Lee, B. Reinhart, S. P. Ertem, E. B. Coughlin, Y. Ren, T. R. Walsh, B. A. Bunker, *ACS Nano* **2016**, 10, 8645.
- [50] Y. Xia, X. Xia, H. C. Peng, *J. Am. Chem. Soc.* **2015**, 137, 7947.
- [51] K. Pappert, *Ph.D. Thesis*, University of Duisburg-Essen **2019**.
- [52] J. G. Mattei, P. Grammatikopoulos, J. L. Zhao, V. Singh, J. Vernieres, S. Steinhauer, A. Porkoyich, E. Danielson, K. Nordlund, F. Djurabekova, M. Sowwan, *Chem. Mater.* **2019**, 31, 2151.
- [53] R. Huang, G. F. Shao, Y. H. Wen, S. G. Sun, *Phys. Chem. Chem. Phys.* **2014**, 16, 22754.
- [54] A. Zaleska-Medynska, M. Marchelek, M. Diak, E. Grabowska, *Adv. Colloid Interface Sci.* **2016**, 229, 80.
- [55] a) W. Haiss, N. T. Thanh, J. Aveyard, D. G. Fernig, *Anal. Chem.* **2007**, 79, 4215; b) V. Amendola, M. Meneghetti, *J. Phys. Chem. C* **2009**, 113, 4277; c) L. M. Liz-Marzan, A. P. Philipse, *J. Phys. Chem.* **1995**, 99, 15120; d) C. Mirkin, R. Letsinger, R. Mucic, J. Storhoff, *Nature* **1996**, 382, 607; e) S. Underwood, P. Mulvaney, *Langmuir* **1994**, 10, 3427; f) S. Link, M. B. Mohamed, M. A. El-Sayed, *J. Phys. Chem. B* **1999**, 103, 3073; g) M. R. Jones, K. D. Osberg, R. J. Macfarlane, M. R. Langille, C. A. Mirkin, *Chem. Rev.* **2011**, 111, 3736; h) S. Mandal, P. R. Selvakannan, R. Pasricha, M. Sastry, *J. Am. Chem. Soc.* **2003**, 125, 8440.
- [56] J. A. Creighton, D. G. Eadon, *J. Chem. Soc., Faraday Trans.* **1991**, 87, 3881.
- [57] a) M. J. Hostetler, J. E. Wingate, C. J. Zhong, J. E. Harris, R. W. Vachet, M. R. Clark, J. D. Londono, S. J. Green, J. J. Stokes, G. D. Wignall, G. L. Glish, M. D. Porter, N. D. Evans, R. W. Murray, *Langmuir* **1998**, 14, 17; b) A. Vincenzo, P. Roberto, F. Marco, M. M. Onofrio, I. Maria Antonia, *J. Phys.: Condens. Matter* **2017**, 29, 203002.
- [58] a) S. A. Diaz, D. A. Hastman, I. L. Medintz, E. Oh, *J. Mater. Chem. B* **2017**, 5, 7907; b) Y. Y. Huang, L. Fuksman, J. Zheng, *Dalton Trans.* **2018**, 47, 6267.
- [59] a) M. Kopp, S. Kollenda, M. Eppe, *Acc. Chem. Res.* **2017**, 50, 1383; b) C. M. Beddoes, C. P. Case, W. H. Briscoe, *Adv. Colloid Interface Sci.* **2015**, 218, 48; c) L. A. Dykman, N. G. Khlebtsov, *Chem. Rev.* **2014**, 114, 1258; d) L. Yang, L. Shang, G. U. Nienhaus, *Nanoscale* **2013**, 5, 1537; e) I. Canton, G. Battaglia, *Chem. Soc. Rev.* **2012**, 41, 2718; f) G. Sahay, D. Y. Alakhova, A. V. Kabanov, *J. Controlled Release* **2010**, 145, 182.
- [60] a) G. A. Sotiriou, S. E. Pratsinis, *Environ. Sci. Technol.* **2010**, 44, 5649; b) A. Panacek, M. Kolar, R. Vecerova, R. Prucek, J. Soukupova, V. Krystof, P. Hamal, R. Zboril, L. Kvitek, *Biomaterials* **2009**, 30, 6333; c) S. Galdiero, A. Falanga, M. Vitiello, M. Cantisani, V. Marra, M. Galdiero, *Molecules* **2011**, 16, 8894; d) Y. Zhou, Y. Kong, S. Kundu, J. D. Cirillo, H. Liang, *J. Nanobiotechnol.* **2012**, 10, 9.

- [61] A. Rostek, M. Breisch, K. Pappert, K. Loza, M. Heggen, M. Köller, C. Sengstock, M. Epple, *Beilstein J. Nanotechnol.* **2018**, 9, 2763.
- [62] a) S. Grade, J. Eberhard, J. Jakobi, A. Winkel, M. Stiesch, S. Barcikowski, *Gold Bull.* **2014**, 47, 83; b) A. Hahn, J. Fuhlrott, A. Loos, S. Barcikowski, *J. Nanopart. Res.* **2012**, 14, 686; c) S. Ristig, S. Chernousova, W. Meyer-Zaika, M. Epple, *Beilstein J. Nanotechnol.* **2015**, 6, 1212.
- [63] M. Breisch, V. Grasmik, K. Loza, K. Pappert, A. Rostek, N. Ziegler, A. Ludwig, M. Heggen, M. Epple, J. C. Tiller, T. A. Schildhauer, M. Koller, C. Sengstock, *Nanotechnology* **2019**, 30, 10.
- [64] a) S. M. Roopan, T. V. Surendra, G. Elango, S. H. S. Kumar, *Appl. Microbiol. Biotechnol.* **2014**, 98, 5289; b) K. M. Rice, G. K. Ginjupalli, N. Manne, C. B. Jones, E. R. Blough, *Nanotechnology* **2019**, 30, 372001.
- [65] a) A. Abuayyash, N. Ziegler, J. Gessmann, C. Sengstock, T. A. Schildhauer, A. Ludwig, M. Köller, *Adv. Eng. Mater.* **2018**, 20, 1700493; b) M. Koeller, P. Bellova, S. M. Javid, Y. Motemani, C. Khare, C. Sengstock, K. Tschulik, T. A. Schildhauer, A. Ludwig, *Mater. Sci. Eng. C* **2017**, 74, 536; c) A. El Arrassi, P. Bellova, S. Memar Javid, Y. Motemani, C. Khare, C. Sengstock, M. Köller, A. Ludwig, K. Tschulik, *ChemElectroChem* **2017**, 4, 1975.
- [66] M. Miernicki, T. Hofmann, I. Eisenberger, F. von der Kammer, A. Praetorius, *Nat. Nanotechnol.* **2019**, 14, 208.
- [67] a) L. C. Liu, A. Corma, *Chem. Rev.* **2018**, 118, 4981; b) G. Prieto, H. Tuysuz, N. Duyckaerts, J. Knossalla, G. H. Wang, F. Schuth, *Chem. Rev.* **2016**, 116, 14056; c) S. Navalon, H. Garcia, *Nanomaterials* **2016**, 6, E123; d) J. Li, T. Zhao, T. Chen, Y. Liu, C. N. Ong, J. Xie, *Nanoscale* **2015**, 7, 7502; e) M. B. Gawande, A. Goswami, T. Asefa, H. Guo, A. V. Biradar, D. L. Peng, R. Zboril, R. S. Varma, *Chem. Soc. Rev.* **2015**, 44, 7540.
- [68] a) M. Jorgensen, H. Gronbeck, *ACS Catal.* **2019**, 9, 8872; b) M. H. Shao, Q. W. Chang, J. P. Dodelet, R. Chenitz, *Chem. Rev.* **2016**, 116, 3594; c) M. C. Luo, S. J. Guo, *Nat. Rev. Mater.* **2017**, 2, 17059; d) K. Kwak, D. Lee, *Acc. Chem. Res.* **2019**, 52, 12; e) Q. Shao, P. T. Wang, X. Q. Huang, *Adv. Funct. Mater.* **2019**, 29, 1806419.
- [69] M. Carmo, D. L. Fritz, J. Mergel, D. Stolten, *Int. J. Hydrogen Energy* **2013**, 38, 4901.
- [70] H. A. Gasteiger, N. M. Marković, *Science* **2009**, 324, 48.
- [71] T. Pingel, S. Fouladvand, M. Heggen, R. E. Dunin-Borkowski, W. Jäger, P. Westenberger, D. Phifer, J. McNeil, M. Skogl, H. Grönbeck, E. Olsson, *ChemCatChem* **2017**, 9, 3544.
- [72] J. Xu, S. Murphy, D. Xiong, R. Cai, X. Wei, M. Heggen, E. Barborini, S. Vinati, R. E. Dunin-Borkowski, R. E. Palmer, L. Liu, *ACS Appl. Energy Mater.* **2018**, 1, 3013.
- [73] a) S. Prabhudev, M. Bugnet, C. Bock, G. A. Botton, *ACS Nano* **2013**, 7, 6103; b) P. Strasser, S. Koh, T. Anniyev, J. Greeley, K. More, C. Yu, Z. Liu, S. Kaya, D. Nordlund, H. Ogasawara, M. F. Toney, A. Nilsson, *Nat. Chem.* **2010**, 2, 454.
- [74] V. R. Stamenkovic, B. Fowler, B. S. Mun, G. Wang, P. N. Ross, C. A. Lucas, N. M. Marković, *Science* **2007**, 315, 493.
- [75] a) V. R. Stamenkovic, B. S. Mun, K. J. J. Mayrhofer, P. N. Ross, N. M. Markovic, *J. Am. Chem. Soc.* **2006**, 128, 8813; b) I. E. L. Stephens, A. S. Bondarenko, F. J. Perez-Alonso, F. Calle-Vallejo, L. Bech, T. P. Johansson, A. K. Jepsen, R. Frydendal, B. P. Knudsen, J. Rossmeisl, I. Chorkendorff, *J. Am. Chem. Soc.* **2011**, 133, 5485.
- [76] a) X. Huang, Z. Zhao, L. Cao, Y. Chen, E. Zhu, Z. Lin, M. Li, A. Yan, A. Zettl, Y. M. Wang, X. Duan, T. Mueller, Y. Huang, *Science* **2015**, 348, 1230; b) V. Beermann, M. Gocyla, E. Willinger, S. Rudi, M. Heggen, R. E. Dunin-Borkowski, M. G. Willinger, P. Strasser, *Nano Lett.* **2016**, 16, 1719.
- [77] M. Alesker, M. Page, M. Shviro, Y. Paska, G. Gershinsky, D. R. Dekel, D. Zitoun, *J. Power Sources* **2016**, 304, 332.
- [78] F. Schüth, R. Palkovits, R. Schlögl, D. S. Su, *Energy Environ. Sci.* **2012**, 5, 6278.
- [79] A. Borodzinski, G. C. Bond, *Catal. Rev.: Sci. Eng.* **2006**, 48, 91.
- [80] M. S. Kamal, A. S. Razzak, M. M. Hossain, *Atmos. Environ.* **2016**, 140, 117.
- [81] G. J. Hutchings, J. K. Edwards, *Front. Nanosci.* **2012**, 3, 249.
- [82] M. M. Montemore, E. D. Cubuk, J. E. Klobas, M. Schmid, R. J. Madix, C. M. Friend, E. Kaxiras, *Phys. Chem. Chem. Phys.* **2016**, 18, 26844.
- [83] D. Liu, Z. Y. Gao, X. C. Wang, J. Zeng, Y. M. Li, *Appl. Surf. Sci.* **2017**, 426, 194.
- [84] M. J. Li, D. J. Cheng, *J. Phys. Chem. C* **2013**, 117, 18746.
- [85] C. Goyhenex, L. Piccolo, *Phys. Chem. Chem. Phys.* **2017**, 19, 32451.
- [86] P. N. Duchesne, Z. Y. Li, C. P. Deming, V. Fung, X. J. Zhao, J. Yuan, T. Regier, A. Aldalbahi, Z. Almarhoon, S. W. Chen, D. E. Jiang, N. F. Zheng, P. Zhang, *Nat. Mater.* **2018**, 17, 1033.
- [87] H. Li, L. Luo, P. Kunal, C. S. Bonifacio, Z. Y. Duan, J. C. Yang, S. M. Humphrey, R. M. Crooks, G. Henkelman, *J. Phys. Chem. C* **2018**, 122, 2712.